

CoMPaSS: Enhancing Spatial Understanding in Text-to-Image Diffusion Models

Gaoyang Zhang^{1,2*}

blurgy@zju.edu.cn

Bingtao Fu²

bingtaofu@vivo.com

Qingnan Fan²

fqnchina@gmail.com

Qi Zhang²

nwpuzhang@gmail.com

Runxing Liu²

runxingliu13@gmail.com

Hong Gu²

guhong@vivo.com

Huaqi Zhang²

zhanghuaqi@vivo.com

Xinguo Liu^{1†}

xinguoliu@zju.edu.cn

¹State Key Lab of CAD&CG, Zhejiang University

²vivo Mobile Communication Co. Ltd

Abstract

Text-to-image (T2I) diffusion models excel at generating photorealistic images, but commonly struggle to render accurate spatial relationships described in text prompts. We identify two core issues underlying this common failure: 1) the ambiguous nature of spatial-related data in existing datasets, and 2) the inability of current text encoders to accurately interpret the spatial semantics of input descriptions. We address these issues with CoMPaSS, a versatile training framework that enhances spatial understanding of any T2I diffusion model. CoMPaSS solves the ambiguity of spatial-related data with the Spatial Constraints-Oriented Pairing (SCOP) data engine, which curates spatially-accurate training data through a set of principled spatial constraints. To better exploit the curated high-quality spatial priors, CoMPaSS further introduces a Token ENcoding ORDERing (TENOR) module to allow better exploitation of high-quality spatial priors, effectively compensating for the shortcoming of text encoders. Extensive experiments on four popular open-weight T2I diffusion models covering both UNet- and MMDiT-based architectures demonstrate the effectiveness of CoMPaSS by setting new state-of-the-arts with substantial relative gains across well-known benchmarks on spatial relationships generation, including VISOR (+98%), T2I-CompBench Spatial (+67%), and GenEval Position (+131%). Code will be available at <https://github.com/blurgy/CoMPaSS>.

1. Introduction

Recent advancements in text-to-image (T2I) diffusion models [40, 41, 44] have transformed visual content creation and significantly shaped the modern digital life [1, 30, 43].

*Work done during internship at vivo.

†Corresponding author, supported by NSFC (No. 62032011).

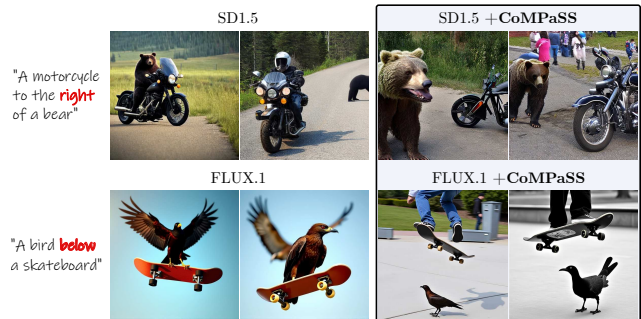


Figure 1. CoMPaSS enables existing T2I diffusion models to generate spatial configurations that are *unlikely to occur naturally and unseen during training* by improving their spatial understanding.

These models are capable of synthesizing photorealistic images with remarkable details [9], and are now widely applied across a range of creative and practical tasks [16, 29, 37, 42]. Despite these advancements, however, a key limitation persists: today’s diffusion models frequently fail to correctly render spatial relationships described in text. For example, when given seemingly simple spatial configurations like “a motorcycle to the right of a bear”, or “a bird below a skateboard”, models that excel in realism often struggle to accurately capture these spatial relationships (Fig. 1 left).

Given that T2I diffusion models have shown significant capability in encoding abstract attributes such as aesthetic style and quality [9, 11, 36, 41], their consistent failure in handling spatial relationships warrants closer examinations. We consider that the limitation stems from *how spatial priors are organized* within the training data, and *how these priors are represented* to the diffusion model.

To better understand this limitation, we conduct a thorough investigation covering the data characteristics during training, and the language representation during generation. Our analysis identified two core issues underlying this spa-

tial understanding deficiency. **First**, the organization of spatial related data in widely-used image-text datasets including LAION [45, 46], CC-12m [2], and COCO [27] is severely flawed. As shown in Fig. 2, spatial descriptions appear frequently ambiguous due to various reasons, such as inconsistent frame of reference, or non-spatial usage of spatial terms. This inevitably leads to the spatial terms being interpreted by the diffusion model as ambiguous. **Second**, commonly used text encoders including CLIP [7, 38] and T5 [39] consistently fail to preserve spatial relationships in their embeddings. Through a proxy task where the text encoders are extensively tested to retrieve the spatial equivalent from three prompt variations (Tab. 1), we show that current text encoders struggle to interpret the accurate meanings of spatial descriptions. Furthermore, the two issues compound each other. Even if a text encoder could reliably capture spatial relationships, the lack of consistent and accurate spatial data would still limit model performance. Conversely, even high-quality spatial descriptions would be undermined by the encoder’s inability to interpret them accurately.

To this end, we seek to enhance the spatial understanding of text-to-image generative diffusion models with a comprehensive solution, which we call CoMPaSS (Comprehensive Method for Positional and Spatial Synthesis). Central to our approach is the Spatial Constraints-Oriented Pairing (SCOP) data engine, which extracts object pairs with clear spatial relationships from images, along with their accurate textual descriptions. By enforcing strict criteria for visual prominence, positional clarity, and size balance, SCOP identifies and validates spatial relationships between object pairs through carefully designed spatial constraints. When applied to the COCO [27] training split, SCOP yields a curated set of over 28,000 object pairs, each coupled with spatially-accurate text descriptions of the image content. To better exploit the accurate spatial priors, we additionally introduce Token ENcoding ORDERing (TENOR), a plug-and-play module that enhances the preservation of spatial semantics from text input with explicit token ordering information, effectively compensating for the spatial understanding limitations of current text encoders. TENOR is compatible with any diffusion architecture, adds no extra parameters, and inflicts practically zero inference-time overhead.

Applying CoMPaSS to popular open-weight T2I diffusion models like SD1.4, SD1.5, SD2.1 and FLUX.1 sets new state-of-the-arts with substantial relative gains on well-known benchmarks, including VISOR [15] (+98%), T2I-CompBench Spatial [22] (+67%), and GenEval Position [14] (+131%). In summary, our contributions are three-fold:

- A comprehensive training framework, CoMPaSS, that significantly enhances spatial understanding in T2I diffusion models.

- A systematic data engine, SCOP, that enforces principled constraints to identify and validate unambiguous spatial relationships between object pairs in images, enabling the curation of high-quality spatial training data.
- A parameter-free module, TENOR, that further improves spatial understanding of T2I diffusion models of any architecture, in the meantime adds negligible computational overhead.

2. Related Works

Text-to-image Diffusion Models. Diffusion models have achieved very high-quality and diverse image synthesis in recent years [9, 18, 34, 41]. To allow natural user input through human language, text-conditional diffusion models adopt datasets with large-scale image-text pairs [2, 26, 45, 46], with pre-trained text encoders to bridge the gap between the two modalities. GLIDE [33], DALLE-2 [40], LDM [41], and the Stable-Diffusion family of models [11, 36, 41] employ CLIP [7, 38] for language conditioning. PixArt- α [5], SD3/3.5 [11], and FLUX.1 adopt the pure-language T5 [39] model as their text encoders. Benchmarking the alignment of image content w.r.t. the input text description has been well explored [14, 15, 20–23]. More recently, CoMat [24] leverages image-to-text (I2T) models [25, 28, 48] to identify the overlooked condition information in generated images during training. ParaDiffusion [50] and ELLA [20] explore the use of large language models (LLMs) in T2I diffusion models.

Instead of trying to enhance the language understanding ability by using more advanced text encoders, we seek an orthogonal direction of facilitating text-image alignment with a data engine that ensures accurate spatial alignment between image and text in training data.

Spatial Control in Diffusion Models. Controllable image generation has become a popular research topic recently. Several lines of works, including both training-based and test-time optimization methods have been explored to enhance the spatial controllability of generation. Previous works add image as conditioning input [32, 51, 52] to enable layout control, but add computational overhead to both training and inference processes. Attention-based methods build upon the relation between the text-image attention map and the layout of generated image [16], and improve compositional generation by explicitly supervising the attention maps either during training [49] or at inference-time [4, 6, 35]. However, supervising attention requires explicit target signal for optimization. Although works like [13, 35] automate the generation of target signals with LLMs, optimization on attention maps still inflicts substantial memory and speed penalty. SPRIGHT [3] avoids test-time optimizations by fine-tuning a diffusion model on datasets recaptured with a vision-language model [28], but

requires joint training of the text encoder in addition to the diffusion network, which still adds considerable training overhead.

In contrast to existing works, we propose a network module that improves spatial understanding of T2I diffusion models of any architecture, in the meantime adds no extra parameters and inflicts practically zero computational overheads to either training or inference processes.

3. Approach

We present CoMPaSS, a comprehensive solution for improving spatial understanding in text-to-image diffusion models. In Sec. 3.1, we develop the Spatial Constraints-Oriented Pairing (SCOP) data engine, which extracts object pairs with clear spatial relationships from images, along with their accurate textual descriptions. In Sec. 3.2, we introduce the Token ENcoding ORdering (TENOR) module, a plug-and-play module that enhances the preservation of spatial semantics from text input by incorporating explicit token ordering information.

These components together form a comprehensive approach to improving spatial understanding in text-to-image diffusion models: SCOP provides high-quality spatial priors through carefully curated spatial relationships, while TENOR enables the model to effectively interpret and exploit these spatial priors during generation.

3.1. The SCOP Data Engine

High-quality spatial understanding in generative models requires training data with unambiguous spatial relationships. However, existing text-image datasets often contain problematic spatial descriptions. As shown in Fig. 2, 1) terms like “left” and “right” suffer from perspective ambiguity, referring inconsistently to viewer perspective or object-intrinsic orientation; 2) directional terms are frequently used in non-spatial contexts (e.g. “the right choice”); 3) spatial relationships are often described with missing or incorrect reference objects, making the intended spatial configuration impossible to determine. These issues create significant challenges for models attempting to learn reliable spatial relationships from such data.

We address this limitation through the Spatial Constraints-Oriented Pairing (SCOP) data engine, which identifies and validates spatial relationships between object pairs through carefully designed spatial constraints. As illustrated in Fig. 3, SCOP processes images through three key stages:

1. Relationship Reasoning. The engine begins by identifying all possible pairwise relationships within each image. For every image \mathbf{I} , we first identify all valid object instances $\{O_1, \dots, O_n\}$, where the i -th object O_i is asso-



Figure 2. **Examples highlighting common ambiguities and errors in spatial language annotations from COCO, LAION, and CC-12M datasets.** (a1, a2) inconsistent frame of reference; (b1) non-spatial usage of spatial terms; (b2, c1, c2) missing or incorrect reference objects.

ciated with a bounding box \mathbf{B}_i and its corresponding category label $\text{Category}(\mathbf{B}_i)$. We then enumerate all possible pairs between the identified objects, creating a total of $\binom{n}{2}$ candidate pairs with their respective spatial relationships to evaluate.

2. Spatial Constraints Enforcement. To ensure unambiguous spatial relationships between object pairs in images, we formalize a set of necessary constraints that collectively guarantee visual clarity and semantic validity. For any candidate object pair (O_i, O_j) , we evaluate five constraints:

- **Visual Significance:** Objects must occupy a sufficient portion of the image to ensure their spatial relationship is meaningful:

$$\frac{\text{Area}(\mathbf{B}_i \cup \mathbf{B}_j)}{\text{Area}(\mathbf{I})} > \tau_v. \quad (1)$$

A relatively small value of τ_v ensures the reasoned spatial relationship from last stage is a dominant feature of the image, rather than an incidental arrangement of background elements.

- **Semantic Distinction:** Objects must belong to different categories, *i.e.*:

$$\text{Category}(\mathbf{B}_i) \neq \text{Category}(\mathbf{B}_j). \quad (2)$$

This constraint eliminates ambiguous cases where multiple instances of the same object category could create reference confusion in spatial descriptions.

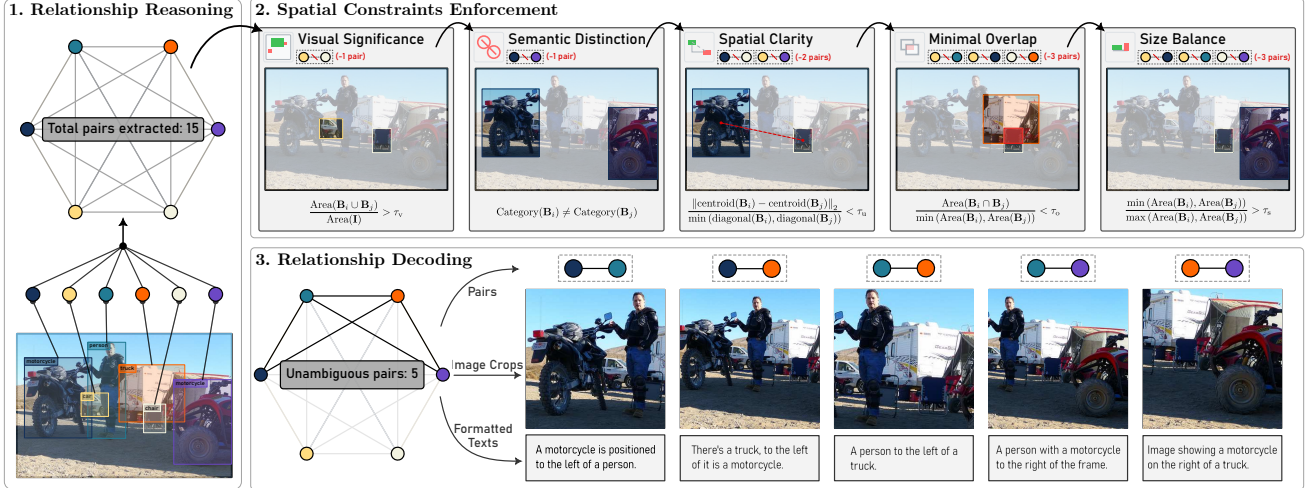


Figure 3. **Overview of the Spatial Constraints-Oriented Pairing (SCOP) data engine.** SCOP first (1) reasons through all possible pairs of objects in image, then (2) identifies and validates spatial relationships between object pairs through carefully designed spatial constraints. Finally, it (3) decodes the extracted unambiguous object pair descriptors into images with accurate spatial descriptions

- **Spatial Clarity:** Objects must be within a reasonable proximity for clear spatial reference. Formally, let $d(i, j) = \|\text{centroid}(\mathbf{B}_i) - \text{centroid}(\mathbf{B}_j)\|_2$, and $l(i, j) = \min(\text{diagonal}(\mathbf{B}_i), \text{diagonal}(\mathbf{B}_j))$, an object pair (O_i, O_j) is said to satisfy spatial clarity when:

$$\frac{d(i, j)}{l(i, j)} < \tau_u, \quad (3)$$

where τ_u upper-bounds the relative distance between O_i and O_j , avoiding ambiguous spatial relationships between far-apart objects.

- **Minimal Overlap:** Objects must maintain sufficient visual separation:

$$\frac{\text{Area}(\mathbf{B}_i \cap \mathbf{B}_j)}{\min(\text{Area}(\mathbf{B}_i), \text{Area}(\mathbf{B}_j))} < \tau_o. \quad (4)$$

The overlap threshold τ_o preserves individual object visibility, while allowing natural spatial configurations like “cup on table” where partial overlap is expected.

- **Size Balance:** The objects in a pair should have comparable visual prominence:

$$\frac{\min(\text{Area}(\mathbf{B}_i), \text{Area}(\mathbf{B}_j))}{\max(\text{Area}(\mathbf{B}_i), \text{Area}(\mathbf{B}_j))} > \tau_s. \quad (5)$$

With this constraint, both objects should contribute similarly to the spatial relationship, preventing cases where one object is too small to serve as a reliable spatial reference.

These constraints effectively filter out ambiguous spatial relationships while preserving natural object interactions, creating a strong foundation for clear and consistent spatial descriptions.

- **3. Relationship Decoding.** For object pairs satisfying all constraints, we adopt a representation system that encodes the spatial relationships with structured descriptors, rather than fixed text. Such descriptors can be decoded into image-text pairs at training time. For example, a descriptor $D = (\text{cup}, \mathbf{B}_{\text{cup}}) \langle \text{above} \rangle (\text{couch}, \mathbf{B}_{\text{couch}})$ can be decoded into $(\mathbf{I}_{\text{roi}}, \mathbf{T})$, where \mathbf{I}_{roi} is a crop of the original image that contains both \mathbf{B}_{cup} and $\mathbf{B}_{\text{couch}}$, and \mathbf{T} is a text prompt formatted from a predefined pool of templates, *e.g.* “a cup on top of a couch”, or “an image of a couch below a cup”, *etc.* Such a decoding process captures the exact positions of the referred objects as well as their reasoned spatial relation, allowing for both accurate relation descriptions and flexible training signals.

The SCOP Dataset. We automate SCOP on the COCO [27] training split to curate a dataset specifically targeted at training T2I models with improved spatial understanding capabilities, covering over 28,000 object pairs across 15,000 images, with well-defined spatial relationships and accurate spatial descriptors. This dataset significantly improves the spatial understanding of T2I diffusion models trained on it, while its size is only a fraction of web-scale datasets (0.004% of LAION-400M [45], or 0.13% of CC-12M [2], showcasing the efficiency and efficacy of the SCOP data engine.

3.2. Token Encoding Ordering Module

Text-to-image diffusion models rely on text encoders to transform natural language descriptions into semantic representations that guide the image generation process. For generation of accurate spatial relationships, these semantic

Table 1. Most similar prompt variation retrieved by different text encoders.

Text Encoder	Used by	F_{text} Space	Most similar prompt variation			Correct
			rephrased	negated relation	swapped entities	
CLIP ViT-L [38]	All	768	1	5088	1231	0.02%
OpenCLIP ViT-H [7]	SD2.1	1024	0	6054	266	0%
OpenCLIP ViT-bigG [7]	SDXL [36], SD3 [11], SD3.5	1280	2	6067	251	0.03%
T5-XXL [39]	SD3 [11], SD3.5, FLUX.1	4096	306	4777	1237	4.84%

representations must preserve the accurate spatial relationships described in the input text. This is the cornerstone for effective spatial understanding of T2I diffusion models.

Analysis of Spatial Understanding. We investigate whether the spatial information is properly represented for the diffusion model to understand it. Our key insight is that if text encoders were able to properly preserve spatial relationships, then *logically equivalent spatial descriptions should yield high similarities* in their encoded representations. A proxy task is designed to quantify this property: given a *base prompt* describing a spatial relationship (e.g., “A to the left of B”), we generate three variations of it: (1) *rephrased*: logically equivalent but differently worded (“B to the right of A”), (2) *negated relation*: substituting the relation phrase with its opposite (“A to the right of B”), and (3) *swapped entities*: exchanging object positions (“B to the left of A”). Theoretically, only the *rephrased* variation should produce an encoding similar to the *base prompt*.

To ensure comprehensive evaluation, we conduct this analysis using all 80 object categories from COCO [27], with four fundamental spatial relationships (“left”, “right”, “above”, “below”), yielding 6,320 prompts. We retrieve the most similar prompt variation according to the similarity between the encoded representations across four text encoders. The results are shown in Tab. 1: even T5-XXL [39] with 11B parameters fails to recognize the logically equivalent variation *over 95% of the time*. Lighter encoders like CLIP [7, 38] show near-complete failures across different model sizes, suggesting that current text encoders do not sufficiently preserve spatial relationships in their encoded representations.

Solution. Based on this analysis, we propose TENOR, a plug-and-play module designed to compensate for the limitations of current text encoders. TENOR operates by augmenting the conditioning text signals with their original token ordering information in attention operations throughout the text-to-image generation process. Unlike the original positional encoding in transformers which only adds positional encodings to the initial token embeddings [47], TENOR explicitly injects the token ordering information

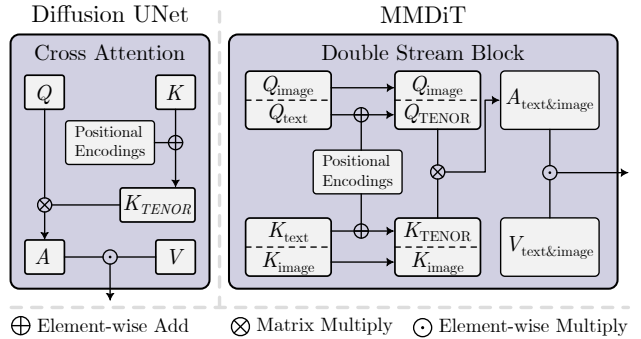


Figure 4. **Overview of Token Encoding Ordering (TENOR).** TENOR injects token ordering information into every text-image attention operation in either UNet- or MMDiT-based diffusion models.

into *every* text-image attention operation in the diffusion model. This design ensures that spatial semantics are actively preserved every time text guidance influences the image generation process.

Implementation and Efficiency. Fig. 4 illustrates the overall process of TENOR. Specifically, in every text-image attention operation in the diffusion model, TENOR adds absolute positional encodings [47] to the K vector for UNet-based models [36, 41], and both K_{text} and Q_{text} for MMDiT-based models [11, 34]. While concurrent approaches have suggested fine-tuning text encoders [3] during training, performing test-time optimizations [4, 6], or incorporating large language models [20, 50], such methods add significant computational overhead either during training or at inference time. In contrast, our solution requires no additional trainable parameters beyond the diffusion model itself, and inflicts practically zero computational penalty at inference time. While adapting TENOR requires a brief fine-tuning phase of the diffusion model, this process is significantly more efficient than training new spatial-aware text encoders. Empirically, we find that this approach substantially improves spatial understanding of both UNet-based models and the MMDiT-based FLUX.1.



Figure 5. **Qualitative results of models enhanced with CoMPaSS.** CoMPaSS enhances the spatial understanding of diffusion models across UNet-based models (SD1.4, SD1.5, SD2.1) and the MMDiT-based FLUX.1.

4. Experiments

4.1. Training Details

We validate the effectiveness of CoMPaSS on four popular open-weight text-to-image diffusion models, where SD1.4, SD1.5, and SD2.1 are based on the UNet architecture [41], and FLUX.1 is based on the MMDiT architecture [11, 34]. For UNet-based diffusion models, we train the entire UNet with a learning rate of $5e-6$. For MMDiT-based FLUX.1, we train a rank-16 LoRA [19] with a learning rate of $1e-5$ due to limited computational resources. All experiments use an effective batch size of 4. Detailed experimental settings can be found in Appendix A.

4.2. Evaluation Metrics

We extensively evaluate CoMPaSS on several well-known benchmarks, which are described below:

- **VISOR** [15] is a specialized benchmark focusing on spatial understanding. It contains 31,680 text descriptions of spatial relationships, and obtains object bounding boxes with an open-vocabulary detector [31] to analyze the generated spatial relationships. Four images are generated for each prompt and success rate is denoted as $VISOR_{uncond}$. Other reported metrics include $VISOR_{cond}$ (rate of accurate spatial relationships given that all the objects are present) and $VISOR_n$, where $n \in \{1, 2, 3, 4\}$ (the probability of at least n out of 4 images correctly depicting the expected spatial relationship).
- **T2I-CompBench** [22] and **GenEval** [14] are two benchmarks designed for comprehensive evaluation of the text-

image alignment capabilities of T2I models. In addition to spatial-related evaluations, they provide methodologies for assessing correctness of attribute binding, non-spatial relationships, and counting. We use them to evaluate the performance impact of CoMPaSS on tasks other than spatial understanding.

- **Fréchet Inception Distance (FID)** [17] and **CLIP Maximum Mean Discrepancy (CMMD)** [23] estimate the fidelity of images generated from T2I models. FID estimates the photorealism of generated images. CMMD is an estimator of image quality that aligns better with human preferences and aims to account for some of the limitations of FID. We report them both.

4.3. Main Results

Spatial Understanding. We evaluate spatial relationship generation accuracy across multiple benchmarks and report them in Tab. 2. Adding CoMPaSS to existing diffusion models sets new state-of-the-art across all spatial-related metrics. Notably, with the best open-weight diffusion model FLUX.1, CoMPaSS obtains substantial relative gains on VISOR (+98%), T2I-CompBench Spatial (+67%), and GenEval Position (131%). As evident in Fig. 5, while existing models often struggle with spatial relationships, CoMPaSS effectively addresses these limitations even on novel spatial configurations unseen during training, demonstrating significant boosts in spatial understanding.

General Generation Capability and Fidelity. Apart from spatial-related metrics, we evaluate other tasks in the

Table 2. **Comparing models enhanced with CoMPaSS and their base models on various spatial-related benchmarks.** CoMPaSS sets new state-of-the-arts with substantial gains on every spatial-related benchmark, including VISOR [15], T2I-CompBench Spatial [22] (T. Spatial), and Geneval Position [14] (G. Position).

Method	VISOR (%)						T. Spatial	G. Position
	uncond	cond	1	2	3	4		
SD1.4	18.81	62.98	46.60	20.11	6.89	1.63	0.12	0.03
SD1.4 +CoMPaSS	57.41	87.58	83.23	67.53	49.99	28.91	0.34	0.46
SD1.5	17.58	61.08	43.65	18.62	6.49	1.57	0.08	0.04
SD1.5 +CoMPaSS	61.46	93.43	86.55	72.13	54.64	32.54	0.35	0.54
SD2.1	30.25	63.24	64.42	35.74	16.13	4.70	0.13	0.07
SD2.1 +SPRIGHT [3]	43.23	71.24	71.78	51.88	33.09	16.15	0.21	0.11
SD2.1 +CoMPaSS	62.06	90.96	85.02	71.29	56.03	35.90	0.32	0.51
FLUX.1	37.96	66.81	64.00	44.18	28.66	14.98	0.18	0.26
FLUX.1 +CoMPaSS	75.17	93.22	91.73	83.31	72.21	53.41	0.30	0.60

Table 3. **Comparison of image fidelity metrics on FID [17] and CMMD [23].**

Method	FID↓	CMMD↓
SD1.4	13.20	0.5618
SD1.4 +CoMPaSS	10.67	0.3313
SD1.5	12.82	0.5548
SD1.5 +CoMPaSS	10.89	0.3235
SD2.1	21.65	0.6472
SD2.1 +SPRIGHT [3]	16.15	0.512
SD2.1 +CoMPaSS	16.96	0.4083
FLUX.1	27.96	0.8737
FLUX.1 +CoMPaSS	26.40	0.6859

Geneval [14] and T2I-CompBench [22] benchmarks, and image fidelity scores on FID [17] and CMMD [23]. The results are reported in Tabs. 3 and 5. CoMPaSS exclusively improves spatial-related performance, while improving the overall alignment scores and image fidelity. We conjecture that in the base models, the spatial terms were entangled with unrelated semantics due to severely flawed data and unclear representation. By exclusively disentangling the spatial terms, the model also learns to better understand other aspects of language, resulting in improvements on other tasks.

4.4. Ablation Studies

In the following, we conduct controlled experiments on SD1.5 (most popular and accessible UNet-based diffusion model) and FLUX.1-dev (a state-of-the-art diffusion model based on the MMDiT architecture) to better understand how each component contributes to generation performance. We

Table 4. **Ablation studies of each component of CoMPaSS.** (i) original models; (ii) trained with the SCOP dataset described in Sec. 3.1; (iii) our full method. T2I-CompBench Spatial (T. Spatial) and Geneval Position (G. Pos) scores are reported.

Setting	Model	Components		T. Spatial	G. Pos.
		SCOP	TENOR		
(i)	SD1.5			0.08	0.04
(ii)	SD1.5	✓		0.32	0.39
(iii)	SD1.5	✓	✓	0.35	0.54
(i)	FLUX.1			0.18	0.26
(ii)	FLUX.1	✓		0.29	0.56
(iii)	FLUX.1	✓	✓	0.30	0.60

report the spatial accuracy metrics under various settings in Tab. 4.

Effect of SCOP. Comparing settings (i) and (ii) within each model reveals that SCOP alone contributes substantially to the spatial understanding of diffusion models. This finding is in line with our initial motivation, where we identified that one of the main reasons current models are failing spatial-related generations is that current datasets yield severely flawed spatial-related image-text data. It also confirms that SCOP is able to curate a set of high-quality data that directly contributes to the spatial understanding of diffusion models.

Effect of TENOR. Tab. 4 shows that our full method (setting (iii) within each model) further improves the spatial accuracy. We prompt the models with text descriptions unseen during training, and compare the generation results with setting (ii). The results are shown in Fig. 6. While SCOP

Table 5. Evaluation results of general generation capabilities across a wide range of tasks on GenEval [14] and T2I-CompBench [22]. CoMPaSS exclusively improves spatial-related performance, while improving the overall alignment scores.

Method	T2I-CompBench					GenEval						
	Color	Shape	Texture	Spatial	Non-Spatial	Position	Single O.	Two O.	Counting	Colors	Attr.	Overall
SD1.4	0.38	0.36	0.42	0.12	0.31	0.03	0.98	0.41	0.34	0.74	0.06	0.43
SD1.4 +CoMPaSS	0.49	0.43	0.53	0.34	0.31	0.46	0.99	0.68	0.34	0.73	0.17	0.56
SD1.5	0.38	0.37	0.42	0.08	0.31	0.04	0.96	0.38	0.36	0.75	0.06	0.42
SD1.5 +CoMPaSS	0.50	0.43	0.52	0.35	0.31	0.54	0.99	0.69	0.34	0.72	0.15	0.57
SD2.1	0.51	0.42	0.49	0.13	0.31	0.07	0.98	0.51	0.44	0.85	0.17	0.50
SD2.1 +SPRIGHT [3]	-	-	-	0.21	-	0.11	0.99	0.59	0.49	0.85	0.15	0.51
SD2.1 +CoMPaSS	0.55	0.43	0.54	0.32	0.30	0.51	0.99	0.69	0.20	0.71	0.15	0.54
FLUX.1	0.69	0.48	0.63	0.18	0.31	0.26	0.92	0.77	0.71	0.66	0.27	0.60
FLUX.1 +CoMPaSS	0.83	0.59	0.71	0.30	0.32	0.60	0.99	0.87	0.71	0.80	0.76	0.76



Figure 6. Ablation study on the TENOR module. TENOR helps the model to gain better generalization capability beyond training data.

provides rich and accurate spatial priors, it is only after incorporating TENOR that the model can better generalize to hard unseen spatial configurations. This phenomenon connects closely to our initial finding about the spatial understanding deficiency of popular text encoders in Tab. 1: when the semantic representations of completely opposite text descriptions are indistinguishable, the model is trained to align mixed image signals from seemingly similar text conditions, resulting in poor generalization beyond training data. TENOR compensates this issue by actively injecting token ordering information into every text-image attention operation throughout the diffusion model, disentangling different spatial configurations at the input level, alleviating the model’s burden of distinguishing different spatial terms, as a result achieving better zero-shot generation on unseen settings.

5. Conclusion

We present CoMPaSS, a versatile training framework that enhances spatial understanding of any text-to-image diffusion model. CoMPaSS addresses the problem of ambiguous spatial relationships in datasets through the SCOP data engine, which curates spatially-accurate training data through principled constraints. CoMPaSS additionally uses a parameter-free module, TENOR, that further boosts spatial understanding of T2I diffusion models of any architecture while adding negligible computational overhead. We conduct extensive experiments on four popular open-weight diffusion models, covering both UNet-based models (SD1.4, SD1.5, SD2.1) and the MMDiT-based FLUX.1, and set new state-of-the-art across well-known benchmarks with substantial relative gains, including VISOR [15] (+98%), T2I-CompBench Spatial [22] (+67%), and GenEval Position [14] (+131%).

Importantly, the enhancement in spatial understanding comes without compromising the general generation capabilities or image quality. By addressing a fundamental limitation of current text-to-image diffusion models, we believe CoMPaSS takes an important step towards reliable spatially-accurate image generation, and opens up new possibilities for applications requiring precise spatial control.

References

- [1] James Betker, Gabriel Goh, Li Jing, Tim Brooks, Jianfeng Wang, Linjie Li, Long Ouyang, Juntang Zhuang, Joyce Lee, Yufei Guo, Wesam Manassra, Prafulla Dhariwal, Casey Chu, Yunxin Jiao, and Aditya Ramesh. Improving Image Generation with Better Captions. [1](#)
- [2] Soravit Changpinyo, Piyush Sharma, Nan Ding, and Radu Soricut. Conceptual 12M: Pushing Web-Scale Image-Text Pre-Training To Recognize Long-Tail Visual Concepts, 2021. arXiv:2102.08981. [2](#), [3](#), [4](#)
- [3] Agneet Chatterjee, Gabriela Ben Melech Stan, Estelle Aflalo, Sayak Paul, Dhruva Ghosh, Tejas Gokhale, Ludwig Schmidt, Hannaneh Hajishirzi, Vasudev Lal, Chitta Baral, and Yezhou Yang. Getting it Right: Improving Spatial Consistency in Text-to-Image Models, 2024. arXiv:2404.01197 [cs]. [2](#), [5](#), [7](#), [8](#)
- [4] Hila Chefer, Yuval Alaluf, Yael Vinker, Lior Wolf, and Daniel Cohen-Or. Attend-and-Excite: Attention-Based Semantic Guidance for Text-to-Image Diffusion Models, 2023. arXiv:2301.13826 [cs]. [2](#), [5](#)
- [5] Junsong Chen, Jincheng Yu, Chongjian Ge, Lewei Yao, Enze Xie, Yue Wu, Zhongdao Wang, James Kwok, Ping Luo, Huchuan Lu, and Zhenguo Li. PixArt- α : Fast Training of Diffusion Transformer for Photorealistic Text-to-Image Synthesis, 2023. arXiv:2310.00426. [2](#)
- [6] Minghao Chen, Iro Laina, and Andrea Vedaldi. Training-Free Layout Control with Cross-Attention Guidance, 2023. arXiv:2304.03373 [cs]. [2](#), [5](#)
- [7] Mehdi Cherti, Romain Beaumont, Ross Wightman, Mitchell Wortsman, Gabriel Ilharco, Cade Gordon, Christoph Schuhmann, Ludwig Schmidt, and Jenia Jitsev. Reproducible Scaling Laws for Contrastive Language-Image Learning. pages 2818–2829, 2023. [2](#), [5](#)
- [8] Boris Dayma, Suraj Patil, Pedro Cuenca, Khalid Saifullah, Tanishq Abraham, Phúc Lê Khac, Luke Melas, and Ritorbrata Ghosh. Dall-e mini. <https://github.com/borisdayma/dalle-mini>, 2021. [2](#)
- [9] Prafulla Dhariwal and Alex Nichol. Diffusion Models Beat GANs on Image Synthesis, 2021. arXiv:2105.05233 [cs, stat]. [1](#), [2](#)
- [10] Ming Ding, Wendi Zheng, Wenyi Hong, and Jie Tang. CogView2: Faster and Better Text-to-Image Generation via Hierarchical Transformers. 2022. [2](#)
- [11] Patrick Esser, Sumith Kulal, Andreas Blattmann, Rahim Entezari, Jonas Müller, Harry Saini, Yam Levi, Dominik Lorenz, Axel Sauer, Frederic Boesel, Dustin Podell, Tim Dockhorn, Zion English, Kyle Lacey, Alex Goodwin, Yan-nik Marek, and Robin Rombach. Scaling Rectified Flow Transformers for High-Resolution Image Synthesis, 2024. arXiv:2403.03206 [cs]. [1](#), [2](#), [5](#), [6](#)
- [12] Weixi Feng, Xuehai He, Tsu-Jui Fu, Varun Jampani, Arjun Akula, Pradyumna Narayana, Sugato Basu, Xin Eric Wang, and William Yang Wang. Training-Free Structured Diffusion Guidance for Compositional Text-to-Image Synthesis, 2023. arXiv:2212.05032 [cs]. [2](#)
- [13] Weixi Feng, Wanrong Zhu, Tsu-jui Fu, Varun Jampani, Arjun Akula, Xuehai He, Sugato Basu, Xin Eric Wang, and William Yang Wang. Layoutgpt: Compositional visual planning and generation with large language models. *Advances in Neural Information Processing Systems*, 36, 2024. [2](#)
- [14] Dhruva Ghosh, Hanna Hajishirzi, and Ludwig Schmidt. GenEval: An Object-Focused Framework for Evaluating Text-to-Image Alignment, 2023. arXiv:2310.11513 [cs]. [2](#), [6](#), [7](#), [8](#)
- [15] Tejas Gokhale, Hamid Palangi, Besmira Nushi, Vibhav Vineet, Eric Horvitz, Ece Kamar, Chitta Baral, and Yezhou Yang. Benchmarking Spatial Relationships in Text-to-Image Generation, 2023. arXiv:2212.10015 [cs]. [2](#), [6](#), [7](#), [8](#)
- [16] Amir Hertz, Ron Mokady, Jay Tenenbaum, Kfir Aberman, Yael Pritch, and Daniel Cohen-Or. Prompt-to-Prompt Image Editing with Cross Attention Control, 2022. arXiv:2208.01626 [cs]. [1](#), [2](#)
- [17] Martin Heusel, Hubert Ramsauer, Thomas Unterthiner, Bernhard Nessler, and Sepp Hochreiter. Gans trained by a two time-scale update rule converge to a local nash equilibrium. *Advances in neural information processing systems*, 30, 2017. [6](#), [7](#)
- [18] Jonathan Ho, Ajay Jain, and Pieter Abbeel. Denoising diffusion probabilistic models. *Advances in Neural Information Processing Systems*, 33:6840–6851, 2020. [2](#)
- [19] Edward J. Hu, Yelong Shen, Phillip Wallis, Zeyuan Allen-Zhu, Yuanzhi Li, Shean Wang, Lu Wang, and Weizhu Chen. LoRA: Low-Rank Adaptation of Large Language Models, 2021. arXiv:2106.09685 [cs]. [6](#)
- [20] Xiwei Hu, Rui Wang, Yixiao Fang, Bin Fu, Pei Cheng, and Gang Yu. ELLA: Equip Diffusion Models with LLM for Enhanced Semantic Alignment, 2024. arXiv:2403.05135. [2](#), [5](#)
- [21] Yushi Hu, Benlin Liu, Jungo Kasai, Yizhong Wang, Mari Ostendorf, Ranjay Krishna, and Noah A. Smith. TIFA: Accurate and Interpretable Text-to-Image Faithfulness Evaluation with Question Answering. pages 20406–20417, 2023.
- [22] Kaiyi Huang, Kaiyue Sun, Enze Xie, Zhenguo Li, and Xihui Liu. T2i-compbench: A comprehensive benchmark for open-world compositional text-to-image generation. *Advances in Neural Information Processing Systems*, 36:78723–78747, 2023. [2](#), [6](#), [7](#), [8](#)
- [23] Sadeep Jayasumana, Srikumar Ramalingam, Andreas Veit, Daniel Glasner, Ayan Chakrabarti, and Sanjiv Kumar. Rethinking FID: Towards a Better Evaluation Metric for Image Generation, 2024. arXiv:2401.09603 [cs]. [2](#), [6](#), [7](#)
- [24] Dongzhi Jiang, Guanglu Song, Xiaoshi Wu, Renrui Zhang, Dazhong Shen, Zhuofan Zong, Yu Liu, and Hongsheng Li. CoMat: Aligning Text-to-Image Diffusion Model with Image-to-Text Concept Matching, 2024. arXiv:2404.03653 [cs]. [2](#)

- [25] Junnan Li, Dongxu Li, Caiming Xiong, and Steven Hoi. Blip: Bootstrapping language-image pre-training for unified vision-language understanding and generation. In *International conference on machine learning*, pages 12888–12900. PMLR, 2022. 2
- [26] Youwei Liang, Junfeng He, Gang Li, Peizhao Li, Arseniy Klimovskiy, Nicholas Carolan, Jiao Sun, Jordi Pont-Tuset, Sarah Young, Feng Yang, Junjie Ke, Krishnamurthy Dj Dvijotham, Katie Collins, Yiwen Luo, Yang Li, Kai J. Kohlhoff, Deepak Ramachandran, and Vidhya Navalpakkam. Rich Human Feedback for Text-to-Image Generation, 2024. arXiv:2312.10240 [cs]. 2
- [27] Tsung-Yi Lin, Michael Maire, Serge Belongie, James Hays, Pietro Perona, Deva Ramanan, Piotr Dollár, and C. Lawrence Zitnick. Microsoft COCO: Common Objects in Context. pages 740–755, Cham, 2014. Springer International Publishing. 2, 3, 4, 5, 1
- [28] Haotian Liu, Chunyuan Li, Qingyang Wu, and Yong Jae Lee. Visual Instruction Tuning, 2023. arXiv:2304.08485 [cs]. 2
- [29] Andreas Lugmayr, Martin Danelljan, Andres Romero, Fisher Yu, Radu Timofte, and Luc Van Gool. RePaint: Inpainting using Denoising Diffusion Probabilistic Models, 2022. arXiv:2201.09865 [cs]. 1
- [30] Inc. MidJourney. Midjourney: Ai-powered image generation. <https://www.midjourney.com/>, 2023. Accessed: 2024-04-27. 1
- [31] Matthias Minderer, Alexey Gritsenko, Austin Stone, Maxim Neumann, Dirk Weissenborn, Alexey Dosovitskiy, Aravindh Mahendran, Anurag Arnab, Mostafa Dehghani, Zhuoran Shen, Xiao Wang, Xiaohua Zhai, Thomas Kipf, and Neil Houlsby. Simple Open-Vocabulary Object Detection with Vision Transformers, 2022. arXiv:2205.06230. 6
- [32] Chong Mou, Xintao Wang, Liangbin Xie, Yanze Wu, Jian Zhang, Zhongang Qi, Ying Shan, and Xiaohu Qie. T2I-Adapter: Learning Adapters to Dig out More Controllable Ability for Text-to-Image Diffusion Models, 2023. arXiv:2302.08453 [cs]. 2
- [33] Alex Nichol, Prafulla Dhariwal, Aditya Ramesh, Pranav Shyam, Pamela Mishkin, Bob McGrew, Ilya Sutskever, and Mark Chen. GLIDE: Towards Photorealistic Image Generation and Editing with Text-Guided Diffusion Models, 2022. arXiv:2112.10741. 2
- [34] William Peebles and Saining Xie. Scalable Diffusion Models with Transformers, 2023. arXiv:2212.09748 [cs]. 2, 5, 6
- [35] Quynh Phung, Songwei Ge, and Jia-Bin Huang. Grounded Text-to-Image Synthesis with Attention Refocusing. pages 7932–7942, 2024. 2
- [36] Dustin Podell, Zion English, Kyle Lacey, Andreas Blattmann, Tim Dockhorn, Jonas Müller, Joe Penna, and Robin Rombach. SDXL: Improving Latent Diffusion Models for High-Resolution Image Synthesis, 2023. arXiv:2307.01952. 1, 2, 5
- [37] Ben Poole, Ajay Jain, Jonathan T. Barron, and Ben Mildenhall. DreamFusion: Text-to-3D using 2D Diffusion, 2022. arXiv:2209.14988 [cs, stat]. 1
- [38] Alec Radford, Jong Wook Kim, Chris Hallacy, Aditya Ramesh, Gabriel Goh, Sandhini Agarwal, Girish Sastry, Amanda Askell, Pamela Mishkin, Jack Clark, Gretchen Krueger, and Ilya Sutskever. Learning Transferable Visual Models From Natural Language Supervision, 2021. arXiv:2103.00020 [cs]. 2, 5
- [39] Colin Raffel, Noam Shazeer, Adam Roberts, Katherine Lee, Sharan Narang, Michael Matena, Yanqi Zhou, Wei Li, and Peter J. Liu. Exploring the Limits of Transfer Learning with a Unified Text-to-Text Transformer. *Journal of Machine Learning Research*, 21(140):1–67, 2020. 2, 5
- [40] Aditya Ramesh, Prafulla Dhariwal, Alex Nichol, Casey Chu, and Mark Chen. Hierarchical text-conditional image generation with clip latents. *arXiv preprint arXiv:2204.06125*, 1(2):3, 2022. 1, 2
- [41] Robin Rombach, Andreas Blattmann, Dominik Lorenz, Patrick Esser, and Björn Ommer. High-Resolution Image Synthesis with Latent Diffusion Models, 2022. arXiv:2112.10752 [cs]. 1, 2, 5, 6
- [42] Nataniel Ruiz, Yuanzhen Li, Varun Jampani, Yael Pritch, Michael Rubinstein, and Kfir Aberman. DreamBooth: Fine Tuning Text-to-Image Diffusion Models for Subject-Driven Generation, 2023. arXiv:2208.12242 [cs]. 1
- [43] Inc. Runway AI. Runwayml: Creative ai tools for content creation. <https://runwayml.com/>, 2023. Accessed: 2024-04-27. 1
- [44] Chitwan Saharia, William Chan, Saurabh Saxena, Lala Li, Jay Whang, Emily L. Denton, Kamyar Ghasemipour, Raphael Gontijo Lopes, Burcu Karagol Ayan, and Tim Salimans. Photorealistic text-to-image diffusion models with deep language understanding. *Advances in neural information processing systems*, 35:36479–36494, 2022. 1
- [45] Christoph Schuhmann, Richard Vencu, Romain Beaumont, Robert Kaczmarczyk, Clayton Mullis, Aarush Katta, Theo Coombes, Jenia Jitsev, and Aran Komatsuzaki. LAION-400M: Open Dataset of CLIP-Filtered 400 Million Image-Text Pairs, 2021. arXiv:2111.02114. 2, 3, 4
- [46] Christoph Schuhmann, Romain Beaumont, Richard Vencu, Cade W. Gordon, Ross Wightman, Mehdi Cherti, Theo Coombes, Aarush Katta, Clayton Mullis, Mitchell Wortsman, Patrick Schramowski, Srivatsa R. Kundurthy, Katherine Crowson, Ludwig Schmidt, Robert Kaczmarczyk, and Jenia Jitsev. LAION-5B: An open large-scale dataset for training next generation image-text models. 2022. 2, 3
- [47] Ashish Vaswani, Noam Shazeer, Niki Parmar, Jakob Uszkoreit, Llion Jones, Aidan N. Gomez, \Lukasz Kaiser, and Illia Polosukhin. Attention is all you need. *Advances in neural information processing systems*, 30, 2017. 5
- [48] Jianfeng Wang, Zhengyuan Yang, Xiaowei Hu, Linjie Li, Kevin Lin, Zhe Gan, Zicheng Liu, Ce Liu, and Lijuan Wang. GIT: A Generative Image-to-text Transformer for Vision and Language, 2022. arXiv:2205.14100. 2
- [49] Zirui Wang, Zhizhou Sha, Zheng Ding, Yilin Wang, and Zhuowen Tu. TokenCompose: Text-to-Image Diffusion with Token-level Supervision, 2024. arXiv:2312.03626 [cs]. 2, 1
- [50] Weijia Wu, Zhuang Li, Yefei He, Mike Zheng Shou, Chunhua Shen, Lele Cheng, Yan Li, Tingting Gao, Di Zhang, and Zhongyuan Wang. Paragraph-to-Image Generation with Information-Enriched Diffusion Model, 2023. arXiv:2311.14284. 2, 5

- [51] Hu Ye, Jun Zhang, Sibor Liu, Xiao Han, and Wei Yang. IP-Adapter: Text Compatible Image Prompt Adapter for Text-to-Image Diffusion Models, 2023. [arXiv:2308.06721 \[cs\]](#). [2](#)
- [52] Lvmin Zhang, Anyi Rao, and Maneesh Agrawala. Adding Conditional Control to Text-to-Image Diffusion Models, 2023. [arXiv:2302.05543 \[cs\]](#). [2](#)

Appendix

A. Additional Training Details

A.1. SCOP Dataset Construction

For the SCOP data engine, we empirically determined the optimal threshold values $\{\tau_v, \tau_u, \tau_o, \tau_s\} = \{0.2, 2.0, 0.3, 0.5\}$ through extensive experimentation. We then applied these thresholds to process the COCO training split [27], resulting in the curated SCOP dataset. The initial Relationship Reasoning stage identifies 2,468,858 object pairs with their corresponding spatial relationships. These pairs are then systematically filtered through the Spatial Constraints Enforcement stage, which applies a series of increasingly stringent criteria: Visual Significance (eliminating 1,929,560 pairs), Semantic Distinction (removing 169,973 pairs), Spatial Clarity (filtering out 119,457 pairs), Minimal Overlap (excluding 148,376 pairs), and Size Balance (removing 73,464 pairs), ultimately yielding 28,028 clear and unambiguous object pairs.

During the training phase, the spatial relationships between object pairs is expressed with one of 8 distinct relationship tokens: <left>, <above>, <right>, <below>, <left+above>, <right+above>, <left+below>, and <right+below>. These relationships are determined based on the exact positions of the objects, with occasional random replacements using the <and> token to enhance robustness. For each pair, we select a square region containing both objects, which is then randomly expanded by up to 10% before being cropped to create the final training image paired with its corresponding text description.

A.2. Model Setups

Our experiments are conducted on four diffusion models, including three UNet-based diffusion models SD1.4¹, SD1.5², SD2.1³, and a state-of-the-art MMDiT-based diffusion model FLUX.1-dev⁴.

For the UNet-based models, we discovered that incorporating attention supervision as proposed by [49] significantly enhanced the convergence of the TENOR module. We therefore integrated this supervision across all UNet-based implementations. In contrast, for the FLUX.1 model, we found that the standard denoising loss alone was sufficient to achieve optimal performance. Notably, our best results were achieved with the CoMPaSS-enhanced FLUX.1

¹<https://huggingface.co/CompVis/stable-diffusion-v1-4>

²<https://huggingface.co/stable-diffusion-v1-5/stable-diffusion-v1-5>

³<https://huggingface.co/stabilityai/stable-diffusion-2-1>

⁴<https://huggingface.co/black-forest-labs/FLUX.1-dev>

model, using a rank-16 LoRA checkpoint that requires only ~ 50 MiB on-disk storage, making it highly efficient for practical applications.

Detailed training hyperparameters for all model configurations are provided in Tab. 7.

B. Runtime Performance of TENOR

The TENOR module represents the only potential source of additional computational overhead in our framework CoMPaSS, as it injects token ordering information into each text-image attention operation within the diffusion models. To quantify its impact, we conducted comprehensive benchmarking of inference latency across all model configurations:

Model	Latency @ 512 × 512	Overhead
SD1.4	1.17s ± 3.04ms	
SD1.4 +TENOR	1.18s ± 7.24ms	+0.85%
SD1.5	1.17s ± 2.50ms	
SD1.5 +TENOR	1.19s ± 4.70ms	+1.71%
SD2.1	1.13s ± 2.50ms	
SD2.1 +TENOR	1.18s ± 4.70ms	+4.42%
FLUX.1	17.3s ± 40.6ms	
FLUX.1 +TENOR	17.8s ± 88.8ms	+2.89%

Our measurements demonstrate that the TENOR module has minimal impact on runtime performance, introducing only negligible computational overhead. Even in the most demanding case of the FLUX.1-dev model, the additional time penalty amounts to just 2.89% of the total inference time, making it a highly practical enhancement for real-world applications.

C. More Experimental Results

C.1. Additional Comparisons on VISOR

We present a comprehensive comparison of VISOR metrics against other state-of-the-art models in Tab. 6, demonstrating the superior performance of our approach across various evaluation criteria.

C.2. More Visual Comparisons

To provide a clear visualization of our approach’s effectiveness, we present additional visual comparisons across eight spatial configurations in Figs. 8 to 11. For each prompt, we generate a total of 36 images using different model configurations, offering a comprehensive view of how our method consistently improves spatial understanding across various scenarios and model architectures.

C.3. Ablation Studies on other Models

While Tab. 4 in the main paper presented ablation studies on SD1.5 and FLUX.1, here we extend our analysis to the

Table 6. **Comparison to state-of-the-art models on the VISOR [15] benchmark.** OA stands for “object accuracy”, which is the success rate of the mentioned objects to appear in the image.

Method	uncond	cond	1	2	3	4	OA
GLIDE [33]	1.98	59.06	6.72	1.02	0.17	0.03	3.36
DALLE-mini [8]	16.17	59.67	38.31	17.50	6.89	1.96	27.10
CogView2 [10]	12.17	65.89	33.47	11.43	3.22	0.57	18.47
Structured Diffusion [12]	17.87	62.36	44.70	18.73	6.57	1.46	28.65
DALLE-2 [40]	37.89	59.27	73.59	47.23	23.26	7.49	63.93
SD1.4	18.81	62.98	46.60	20.11	6.89	1.63	29.86
SD1.5	17.58	61.08	43.65	18.62	6.49	1.57	28.79
SD2.1	30.25	63.24	64.42	35.74	16.13	4.70	47.83
SD2.1 +SPRIGHT [3]	43.23	71.24	71.78	51.88	33.09	16.15	60.68
FLUX.1	37.96	66.81	64.00	44.18	28.66	14.98	56.95
SD1.4 +CoMPaSS	57.41	87.58	83.23	67.53	49.99	28.91	65.56
SD1.5 +CoMPaSS	61.46	93.43	86.55	72.13	54.64	32.54	65.78
SD2.1 +CoMPaSS	62.06	90.96	85.02	71.29	56.03	35.90	68.23
FLUX.1 +CoMPaSS	75.17	93.22	91.73	83.31	72.21	53.41	78.64

Table 7. **Hyperparameters used during training.**

Hyperparameter	SD1.4	SD1.5	SD2.1	FLUX.1
AdamW Learning Rate (LR)	5e-6	5e-6	5e-6	1e-4
AdamW β_1	0.9	0.9	0.9	0.9
AdamW β_2	0.999	0.999	0.999	0.999
AdamW ϵ	1e-8	1e-8	1e-8	1e-8
AdamW Weight Decay	1e-2	1e-2	1e-2	1e-2
LR scheduler	Constant	Constant	Constant	Constant
LR warmup steps	0	0	0	20
Training Steps	24,000	24,000	80,000	24,000
Local Batch Size	1	1	1	1
Gradient Accumulation	2	2	2	2
Training GPUs	2×L40S	2×L40S	2×L40S	2×L40S
Training Resolution	512 × 512	512 × 512	512 × 512	512 × 512
Trained Parameters	All parameters of diffusion UNet		LoRA (rank=16) on all DoubleStreamBlocks	
Prompt Dropout Probability	10%	10%	10%	10%

Table 8. **Ablation studies of each component of CoMPaSS.** (i) original models; (ii) trained with the SCOP dataset described in Sec. 3.1 of the main paper; (iii) our full method. T2I-CompBench Spatial (T. Spatial) and GenEval Position (G. Pos) scores are reported.

Setting	Model	Components		T. Spatial	G. Pos.
		SCOP	TENOR		
(i)	SD1.4			0.12	0.03
(ii)	SD1.4	✓		0.29	0.36
(iii)	SD1.4	✓	✓	0.34	0.46
(i)	SD2.1			0.13	0.07
(ii)	SD2.1	✓		0.30	0.36
(iii)	SD2.1	✓	✓	0.32	0.51

other two UNet-based diffusion models SD1.4 and SD2.1 in Tab. 8. The results consistently demonstrate that both components of CoMPaSS contribute to improved spatial understanding across different model architectures.

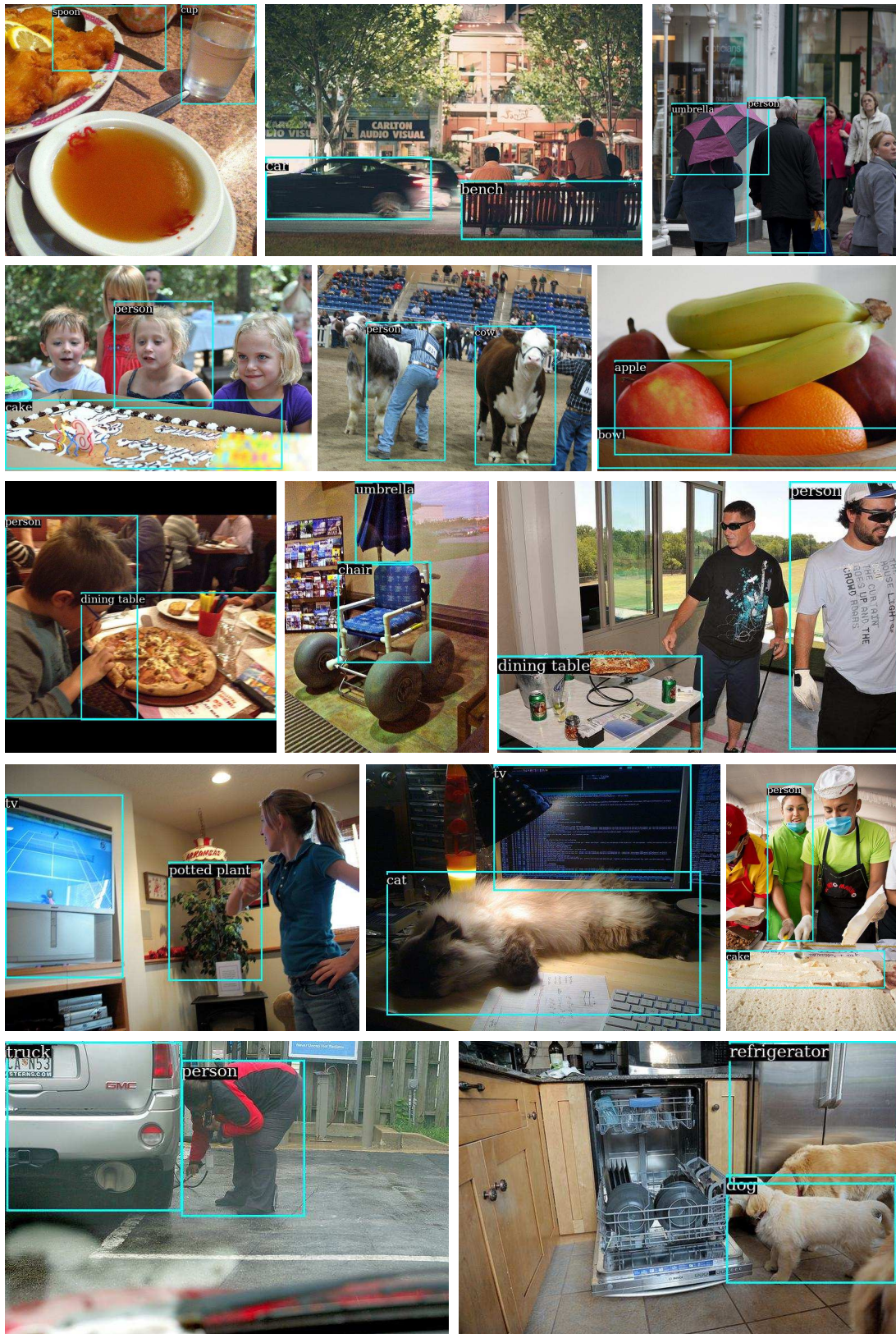
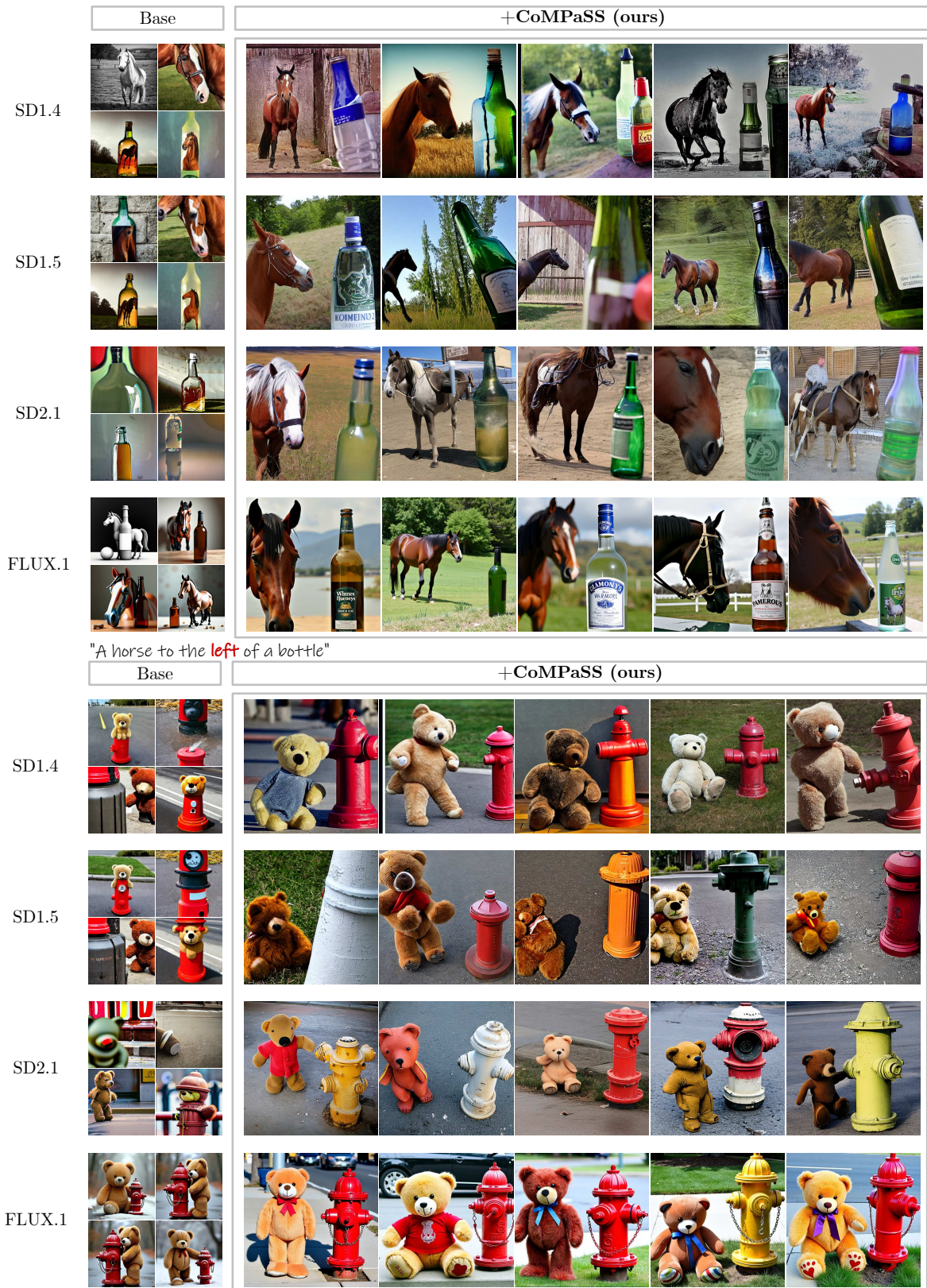
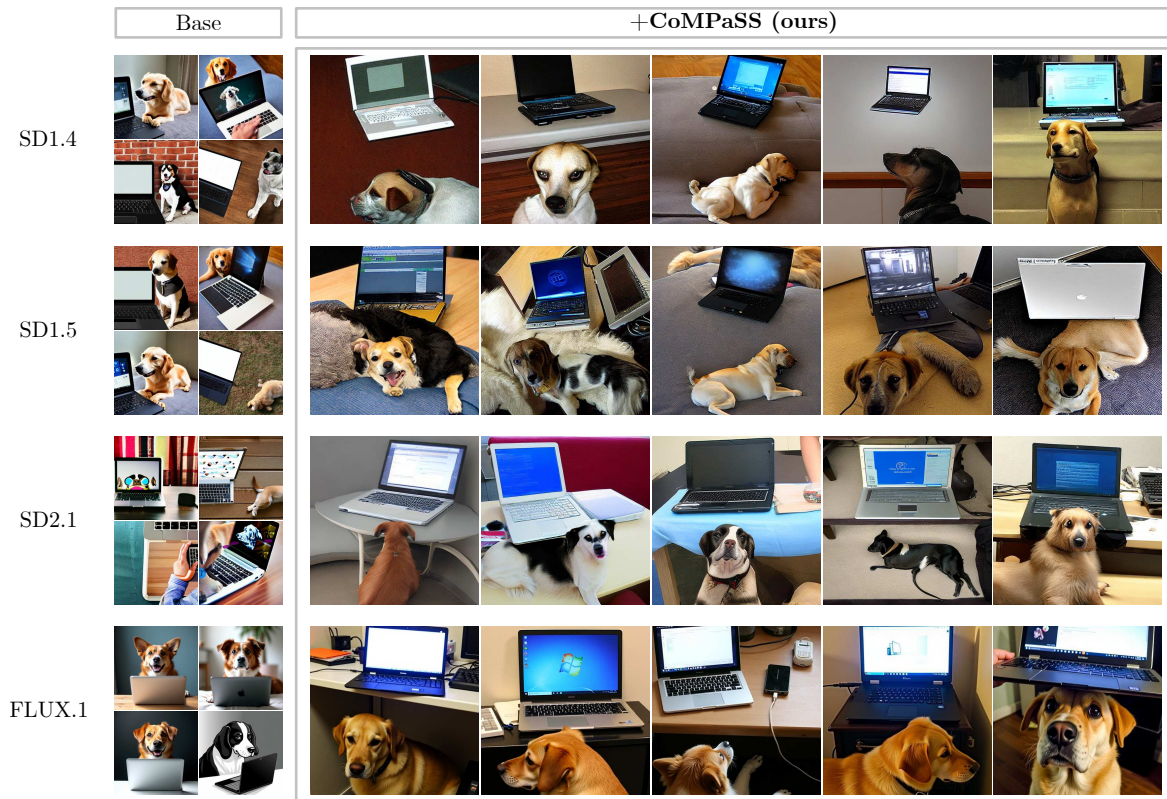


Figure 7. Example object pairs and their corresponding bounding boxes extracted by the SCOP data engine. Each pair satisfies our spatial constraints for Visual Significance, Semantic Distinction, Spatial Clarity, Minimal Overlap, and Size Balance, ensuring unambiguous spatial relationships.



"A teddy bear to the **left** of a fire hydrant"
 Figure 8. **Additional results demonstrating spatial relationship "left"**. Each row shows generations from different models for the same text prompt. The first two columns (16 images) are from baseline models (SD1.4, SD1.5, SD2.1, FLUX.1), while the remaining five columns (20 images) are from their CoMPaSS-enhanced counterparts, showing consistent improvements in spatial understanding.

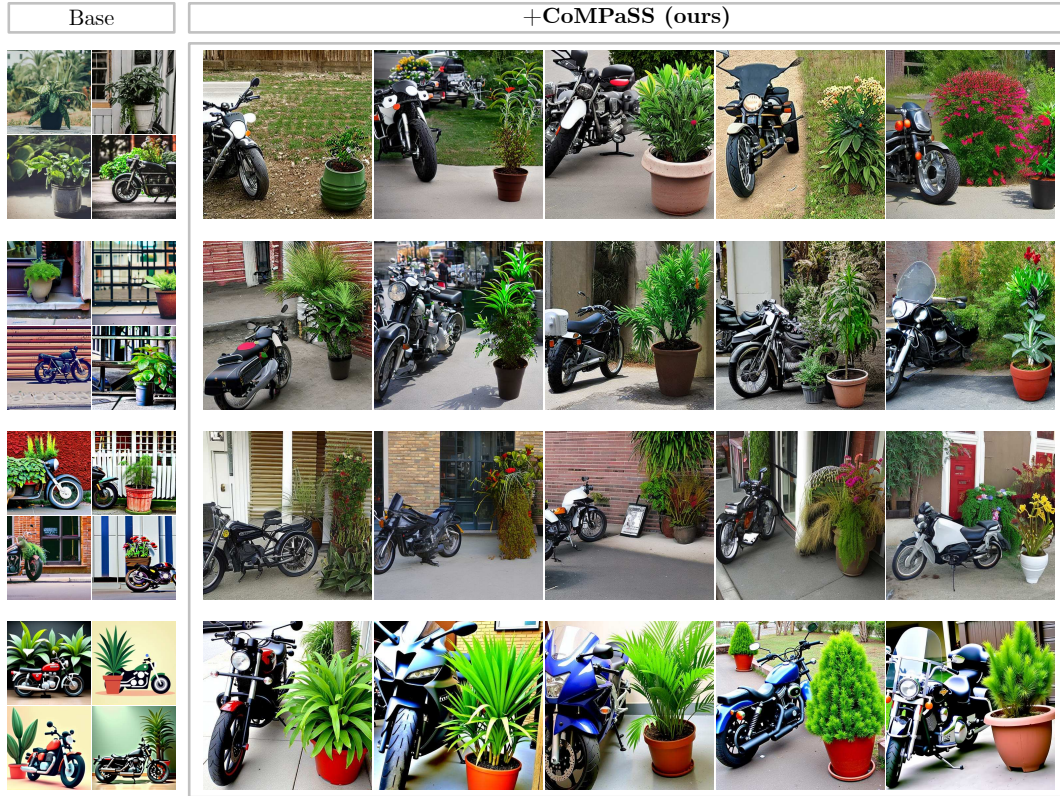


"A laptop *above* a dog"



"A clock *above* an airplane"

Figure 9. **Additional results demonstrating spatial relationship “above”**. Each row shows generations from different models for the same text prompt. The first two columns (16 images) are from baseline models (SD1.4, SD1.5, SD2.1, FLUX.1), while the remaining five columns (20 images) are from their CoMPaSS-enhanced counterparts, showing consistent improvements in spatial understanding.



"A potted plant to the **right** of a motorcycle"



"A bear to the **right** of a truck"

Figure 10. **Additional results demonstrating spatial relationship “right”**. Each row shows generations from different models for the same text prompt. The first two columns (16 images) are from baseline models (SD1.4, SD1.5, SD2.1, FLUX.1), while the remaining five columns (20 images) are from their CoMPaSS-enhanced counterparts, showing consistent improvements in spatial understanding.

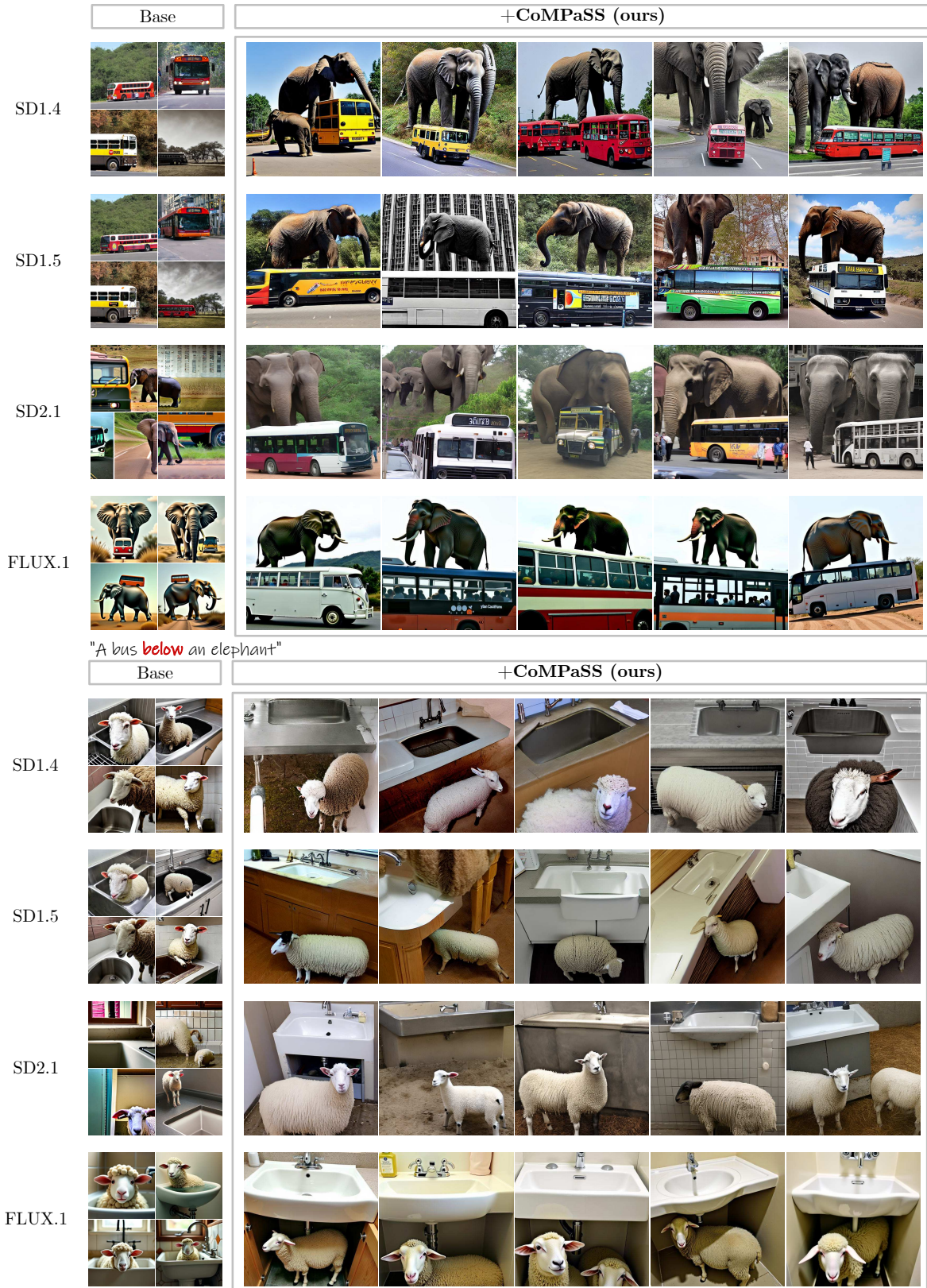


Figure 11. **Additional results demonstrating spatial relationship “below”**. Each row shows generations from different models for the same text prompt. The first two columns (16 images) are from baseline models (SD1.4, SD1.5, SD2.1, FLUX.1), while the remaining five columns (20 images) are from their CoMPaSS-enhanced counterparts, showing consistent improvements in spatial understanding.